We are IntechOpen,
the world's leading publisher of
Open Access books
Built by scientists, for scientists

4,800
Open access books available

122,000
International authors and editors

135M
Downloads

Our authors are among the

154
Countries delivered to

TOP 1%
most cited scientists

12.2%
Contributors from top 500 universities

CLARIVATE ANALYTICS
BOOK CITATION INDEX
INDEXED

WEB OF SCIENCE™

Selection of our books indexed in the Book Citation Index
in Web of Science™ Core Collection (BKCI)

Interested in publishing with us?
Contact book.department@intechopen.com

Numbers displayed above are based on latest data collected.
For more information visit www.intechopen.com

Electron Orbital Contribution in Distance-Dependent STM Experiments

Alexander N. Chaika

Additional information is available at the end of the chapter

Abstract

Scanning tunneling microscopy (STM) is one of the most powerful techniques for the analysis of surface reconstructions at the atomic scale. It utilizes a sharp tip, which is brought close to the surface with a bias voltage applied between the tip and the sample. The value of the tunneling current, flowing between the tip and the sample, is determined by the structure of the surface and the tip, the bias voltage, and the tip-sample distance. By scanning the tip over the surface, a tunneling current map is produced, which reflects the local atomic and electronic structures. This chapter focuses on the role of the tip-surface distance in ultrahigh vacuum STM experiments with atomic and subatomic resolution. At small distances, i.e., comparable with interatomic distances in solids, the interaction between the tip and the surface atoms can modify their electronic structure changing the symmetry of the atomically resolved STM images and producing unusual features at the subatomic scale. These features are related to changes of the relative contribution of different electron orbitals of the tip and the surface atoms at varying distances.

Keywords: atomic resolution, density of states, electron orbital, gap resistance, scanning tunneling microscopy

1. Introduction

The invention of scanning probe microscopy (SPM) [1–3] allowed studying the surface structures with extremely high spatial resolution. The SPM methods use sharp tips, which are ultimately ended with a single atom at the apex, for surface imaging [4–7], fabricating low-dimensional structures from individual atoms and molecules [8–14], studying the physical properties of the nanoobjects [15, 16], and getting the information about the chemical [17, 18] and magnetic

order on surfaces [19–21]. SPM methods are utilized in the fields of physics, chemistry and biology for precise studies of organic and inorganic nanoobjects. The subatomic spatial resolution [22–33] has been achieved during the last decade in the atomic force microscopy (AFM) and scanning tunneling microscopy (STM) experiments.

STM is based on quantum tunneling of electrons from atoms present at the surface of a sample to the front atom of an STM tip (or vice versa) through the vacuum gap. Because of the exponential distance dependence [34], the tunneling current drops approximately by one order of magnitude with every 1 Å increase in the tip-sample separation. Because of the strong distance dependence, more than 90% of the current can be localized on only two, closest to each other, tip and surface atoms. This provides unique spatial resolution of STM, reaching the picometer scale [15, 22–24] and allowing even direct imaging individual electron orbitals at certain tunneling parameters [22–28]. However, the ultimate orbital resolution could rarely be achieved in experiments because of simultaneous contribution of different electron states of the tip and the surface atoms and nonideal geometries of the tips used. Probing particular atomic orbitals with STM is further impeded by possible modifications of the tip and surface electronic structure at very small tunneling gaps (2.0–5.0 Å), generally required for atomically resolved STM imaging.

The role of different electron states and tip-surface distance in high-resolution STM imaging has been discussed since 1980s. Apparently, the first anomalous distance dependence of the STM contrast was reported in reference [35]. Afterward, the distance dependence has been studied in a number of works [22, 23, 27, 28, 36–46]. However, because of complexity of the theoretical calculations for realistic tip-surface systems and experimental studies with precise control of the tunneling gap and the tip state, there is still no detailed knowledge about the role of particular electron orbitals in the distance-dependent STM experiments. This chapter is focused on the experimental and theoretical studies of the role of the tip-sample distance in STM experiments with atomic and subatomic spatial resolution which can pave the way to selective probing particular electron orbitals, controllable chemical analysis at the atomic scale, and surface imaging with picometer lateral resolution.

2. Role of the electron orbitals and tip-surface distance in STM experiments: theory

2.1. Spatial resolution with different atomic orbitals at the tip apex

One of the critical issues of high-resolution STM studies is the lack of reliable information about the tip apex structure, which complicates theoretical calculations and comparison with experimental results. To simplify the calculations, Tersoff and Hamann considered a spherically symmetric s-wave STM tip [47, 48]. In this case, the tunneling current is proportional to the local density of states (DOS) of the surface at the position of the tip, integrated in the energy range defined by the bias voltage. The STM images, calculated using the Tersoff-Hamann model, reflect the surface DOS distribution. This theory has provided a good agreement

between the simulated and experimental images for numerous atomically resolved STM studies.

The ultimate lateral resolution R within the Tersoff-Hamann approach [47] is defined by the formula $R = \sqrt{d \cdot 2k^{-1}}$, where d is the distance between the interacting tip and surface atoms and $k^{-1} \approx 1$ Å. The limit of the lateral resolution for a tip-sample distance of 4.5 Å should be about 3 Å. The theory [47] predicts an enhancement of the spatial resolution with decreasing tip-sample distance but cannot explain the large atomic corrugations in STM images of metal surfaces [49–51] and the experimentally observed sub-Ångström lateral resolution [7, 22–24], even at tunneling gaps in the range of 2.0–2.5 Å. The former can be explained either by the tip and surface atom relaxations [37] or by decisive contribution of higher momentum (l) electron states with nonzero momentum projections on the z-axis ($m \neq 0$ states) [52–56]. For example, calculations by Tersoff and Lang for different tip atoms (Mo, Na, Ca, Si, and C) suggest that atomic corrugations on the same surface can vary by one order of magnitude depending on the relative contribution of the electron states with different values of l and m [52].

To get more general description of the tip structure and to clarify the role of particular electron orbitals in STM imaging, Chen introduced the so-called derivative rule [54], where the tunneling matrix elements, corresponding to individual orbital contributions, are proportional to the z derivatives of the surface atom wave functions at the center of the tip apex atom. The total tunneling current can be calculated by summing up all individual contributions of the electron orbitals with different values of l and m [54]. According to the theory [54, 55], d_z^2 and p_z tip electron states can be responsible for enhanced atomic resolution and large corrugations on metallic surfaces. For the tips having $m = 0$ electron states at the apex, the simulated STM images should correspond to the surface DOS distribution, similar to the s-wave tip. This assumes that the best STM tips should possess either d_z^2 or p_z electron states at the apex. At the same time, the $m \neq 0$ tip states (e.g., d_{xz}, d_{yz}, d_{xy}, and $d_{x^2-y^2}$) can provide enhanced atomic corrugations and intra-atomic effects at small distances [53–56]. For example, d_{xz}, d_{yz}, d_{xy}, and $d_{x^2-y^2}$ electron orbitals at the apex can produce twofold and fourfold split subatomic features, respectively, instead of a single atom at very small tunneling gaps [56]. The dependence of atomic corrugations on the tunneling gap resistance, calculated for different electron orbitals by Sacks [56], suggested that d_z^2 and $m \neq 0$ d-orbitals can produce enhanced corrugations in comparison to the s-state. Furthermore, the corrugations can substantially increase with decreasing gap resistance.

The improvement of the lateral resolution of the SPM to the picometer scale [7, 22–24, 57–60], observation of orbital channels in tunneling conductance [61], and subatomic contrast in SPM experiments [22–32] led to the development of new theories accounting for the distance dependence of the electron orbital contribution [62, 63], energy-dependent combinations of the tip orbitals [64–68], and effects of inter- and intra-atomic interference of the electron orbitals in the tunneling junction [69–73]. Recently, the revised Chen's derivative rule, accounting for the orbital interference effects, has been proposed by Mandi and Palotas [74], who considered the realistic electronic structure and arbitrary spatial orientation of the tip minimizing the computational efforts. Their results showed that the electronic interference effects have a

considerable effect on the STM images. As an example, in certain cases a tip with a mixture of s and p_z electron states can provide even higher spatial resolution than pure p_z-orbital tip [74].

2.2. Electronic structure of realistic tips at small tunneling gaps

Although the developed theories can provide a correlation between experimental and theoretical images in certain cases, they rarely take into account possible interaction-induced changes of the tip orbital structure at very small tunneling gaps. It has been demonstrated recently [62–64, 75] that electronic structure of the transition metal tips and relative weights of different d-orbitals in the tip's DOS near E_F strongly depend on the tip element, tip cluster size, and local environment around the tip. In particular, it has been shown that d_z^2-orbital is more sensitive to the local environment and the tip cluster size than $m \neq 0$ d-orbitals (d_{xz}, d_{yz}, d_{xy}, and $d_{x^2-y^2}$) [63]. The electronic structure of different transition metal tips can nonequally depend on the tip-surface distance [63, 75]; therefore, determination of the most suitable tip for particular surface can be crucial for reaching highest spatial resolution in the experiments. Stimulated by the subatomic resolution AFM experiments [33], Wright and Solares calculated
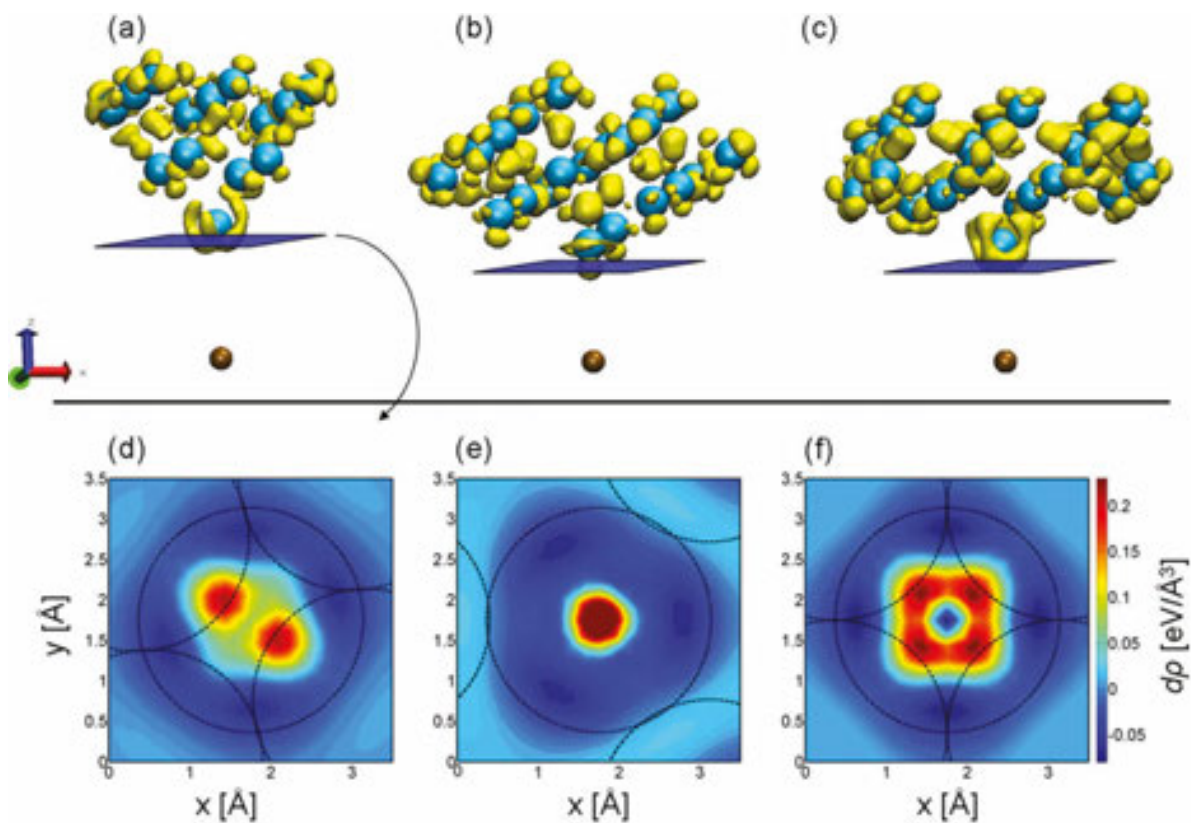

Figure 1. (a–c) The $d\rho = 0.08$ eV/Å^3 isosurface of the change in electron density for the (a) He–W[011], (b) He–W[111], and (c) He–W[001] systems. The helium atom is positioned directly below the front atom of the tip, with a gap of 4.0 Å for the W[011] tip and 3.5 Å for the W[111] and W[001] tips. (d–f) Constant-height slices through the electron density distribution. The relative sizes and positions of the first two layers of the tips' tungsten atoms are drawn as black circles. Reproduced from Reference [75] with permission of IOP.

the electronic structure of the tungsten tips with different crystallographic orientations in proximity to different surface clusters [75–77]. The calculations showed that the experimental SPM images with subatomic resolution [22–24, 33] were, most probably, related to the tip electronic structure, which could become asymmetric at small tip-sample distances because of the tip-sample interaction. The stability of the tungsten tips was found to be dependent on the crystallographic orientation of the apex. In particular, W[001] tip did not substantially relax even at the tip-sample distance of 1.50 Å, while [011]- and [111]-oriented tungsten tips were stable only at gaps above 2.25 and 2.50 Å, respectively. **Figure 1(a)–(c)** shows the isosurfaces of the change in the electron density calculated for the [011]-, [111]-, and [001]-oriented tungsten tips interacting with the helium atom positioned directly below the front atom of the tips [75]. **Figure 1(d)–(f)** illustrates that essentially asymmetric charge density distribution is observed near the front atom of the W[011] and W[001] tips. These areas of increased charge density (dark red color) reveal the twofold and fourfold symmetry representatives of each tip's crystallographic orientation. However, for the W[111] tip, the areas of increased density do not reveal the threefold symmetry proposed from the crystal symmetry consideration [33]. These results suggest that the highest spatial resolution can be achieved in STM experiments using W[111] tips which have symmetrical charge density distribution along the tip axis even at relatively small distances from the surface. In contrast, W[001] and W[011] tips can produce subatomic features at small tip-sample distances [22–24] but can be more suitable for scanning tunneling spectroscopy (STS) experiments demanding high tip stability.

2.3. Role of atomic relaxations at small tip-surface distances

An enhancement of the lateral resolution and atomic corrugations with decreasing tip-surface distance was anticipated from the theories [47, 56] omitting possible relaxations of the interacting tip and surface atoms. Additionally, the topographic contrast in STM experiments can be enhanced at small distances because of the tip and surface atom relaxations reported for the first time almost three decades ago [49]. The role of elastic effects in high-resolution STM experiments on close-packed metal surfaces was thoroughly studied in Ref. [37]. To evaluate possible corrugation enhancement related to atomic relaxations, the simulations were performed on Cu(111) and Al(111) surfaces at different tip configurations and tunneling gaps [37]. The relaxations were found to be substantially stronger for Al(111) because of the higher elasticity of the aluminum surface. As a result, the atomic corrugations in the simulated images of Al(111) increased almost by one order of magnitude (from 10 to 70 pm) with decreasing distance from 600 to 400 pm. The calculations [37] explain the anomalously high corrugation amplitudes observed in numerous STM experiments on metal surfaces. The large outward relaxations of the surface atoms under typical tunneling conditions can lead to atomic corrugations which can hardly be explained from the electron DOS and simplified theoretical considerations [47, 56]. The corrugation enhancement was proved on different metal surfaces; therefore, one can anticipate the validity of the work [37] for other metals, although the effect cannot be so well pronounced as calculated for aluminum surface scanned by an aluminum-terminated tip.

2.4. Reduction in tunneling current channels with decreasing tip-surface distance

First observations of the tunneling current channels associated with different electron orbitals were reported almost two decades ago [61]. However, their role in STM imaging at different gaps is still not clear. Recent theoretical studies showed that relative contributions of different electron orbitals can be substantially modified because of tip-sample interaction changing the tip and surface DOS near E_F [62–64, 75, 78–80]. For example, **Figure 1** demonstrates the distinct asymmetry of the [001]- and [011]-oriented tungsten probes appearing only at small gaps when the overlap of the orbitals of the interacting tungsten and helium atoms takes place [75]. **Figure 2** shows the theoretical calculations demonstrating a drastic reduction of the DOS near E_F associated with the Si(111)7×7 surface atom interacting with the [001]-oriented tungsten tip [79]. The interaction modifies the electronic structure of the surface atom at distances below 4.75 Å, as shown in **Figure 2(d)**. The calculations predict a nonmonotonous dependence of the interaction forces [**Figure 2(b)**] and the tunneling current [**Figure 2(c)**] at these distances. The calculations reveal the exponential current–distance dependence at large distances and drop of tunneling conductance at a distance of 4.75 Å [**Figure 2(c)**]. **Figure 2(b)** and **(c)** demonstrates a correlation between the upward adatom displacement, the decrease of the conductance, and the formation of the chemical bond between the apex atom and the surface adatom. At large tip-sample distances, there is no significant vertical displacement of the adatom [**Figure 2(c)**]. Large upward relaxations of the adatom are observed at the distances of around 5 Å. At the same distances, the short-range chemical force between the tip and the sample changes rapidly
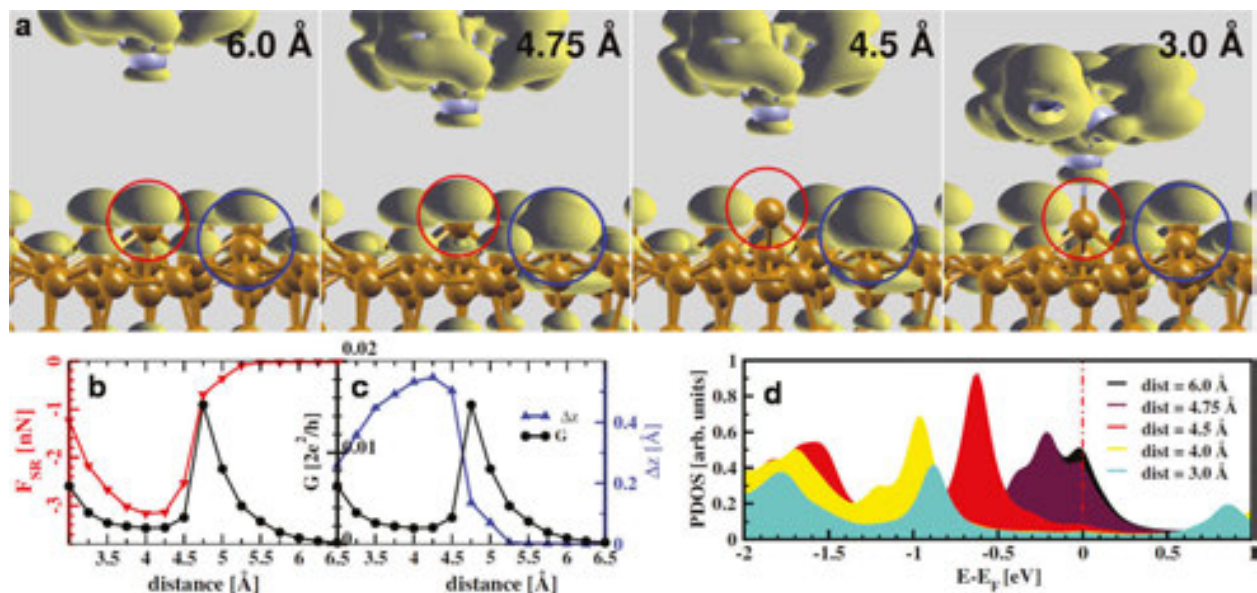

Figure 2. (a) Isosurfaces of electron charge density (the isovalue is 0.08 e/Å^3) integrated in the energy range from E_F to E_F – 0.4 eV, for different tunneling gaps. The probe is placed over the corner adatom in the Si(111)7×7 faulted unit cell. (b) Evolution of the quantum conductance G (right axis) and the atomic force (left axis) as a function of the tip-sample distance. (c) The quantum conductance (left axis) and the vertical adatom displacement (right axis) as a function of the distance. (d) PDOS of the silicon corner adatom as a function of the tip-sample distance. Reproduced from Reference [78] with permission of APS.

[**Figure 2(b)**]. Then, the vertical adatom displacement decreases until it reaches its initial value at a tip-sample distance of 3 Å. The electron DOS isosurfaces calculated for different tip-sample distances [**Figure 2(a)**] show the typical charge density distribution of the Si(111)7×7 surface at 6.0 Å, a charge transfer from the adatom to neighboring surface atoms at 4.75 Å, the suppression of the adatom dangling bond at 4.5 Å, and the chemical bond formation at 3.0 Å that prevents the electron transport between the tip and the surface at small distances. The W[001] tip electronic structure remained practically unchanged in this tip-sample distance range. Note that calculations of Jelinek et al. [78] were carried out at low voltages, corresponding to probing the p_z-states dominating in the Si(111)7×7 surface DOS near E_F. Therefore, it can be assumed that the overlap of the silicon p_z-orbital with the tungsten tip orbitals is responsible for the strong modification of the tunneling current as shown in **Figure 2(d)**. Furthermore, one can expect similar phenomena in other systems where the electron transport occurs through p_z electron orbitals.

Recent theoretical calculations of the tunneling current between an STM tip and a single Cu/Co atom adsorbed on a Cu(001) surface [62] have shown that conductance in these systems can be decomposed into several orbital contributions. The tunneling probabilities of these individual channels can provide the information about the modifications of the adatom's DOS caused by the tip-adatom interaction. The calculations revealed that the d_z^2-orbitals of the interacting atoms in such systems are especially sensitive to the tip-adatom distance because they start to overlap at larger distances. The DOS associated with the $d_{x^2-y^2}$-orbitals starts to decrease at smaller tunneling gaps and the total reduction at distances between 4.0 and 2.5 Å for this orbital is smaller in comparison with that of the d_{xz}-, d_{yz}-, and d_z^2-orbitals. At tip-sample distances exceeding 3.0 Å, the channels contributing to the most of the tunneling current were generally related to hybrids of s- and d_z^2-orbitals. The contribution of $m \neq 0$ electron states increased with decreasing distances.

3. Electron orbital resolution in distance-dependent STM experiments

The first STM images with the atomic orbital resolution were obtained at the beginning of 1980s. For example, typical images of the Si(111)7×7 surface [5] correspond to direct visualization of the p_z surface orbitals. Similar selective visualization of the atomic orbitals at certain tunneling conditions was achieved on other semiconducting surfaces [17]. The control of the orbital contribution on multicomponent metal surfaces is more difficult. Up to date, several STM studies demonstrating subatomic, electron orbital contrast have been published. In several cases, the observed features were related to direct visualization of the electronic structure of the tip atom by more localized surface atomic orbitals [22–28]. However, some STM studies revealed asymmetric subatomic features associated with the $m \neq 0$ electron orbitals of the surface atoms [30, 81]. The STM studies presented in this section can be important for optimizing the tunneling parameters for high-resolution STM imaging and shed light on the gap resistance dependence of atomically resolved STM images and chemical contrast observed on metallic and semiconducting surfaces.

3.1. Tip orbitals resolved using p_z states of the Si(111)7×7 surface atoms

SPM imaging with subatomic resolution was first claimed by Giessibl et al. [31] who reported the AFM images of the Si(111)7×7 reconstruction demonstrating a regular twofold splitting of the surface atomic features. This was explained by direct visualization of the two atomic orbitals of an Si[001] tip atom by the p_z-orbitals of the surface atoms. This is schematically shown in **Figure 3(b)**. Later studies [28] showed that qualitatively the same asymmetric features can be resolved with STM using a silicon-terminated tungsten tip. **Figure 3(a)** demonstrates the change of the contrast in the STM experiments [28] with decreasing tunneling gap resistance. Note that precise structure of the tip apex, responsible for the subatomic contrast in both SPM experiments [28, 31], was unknown because of the tip preparation procedure. Therefore, the origin of the subatomic features in the Si(111)7×7 SPM images was disputed in a number of papers [82–87]. Alternative explanations based on the feedback loop
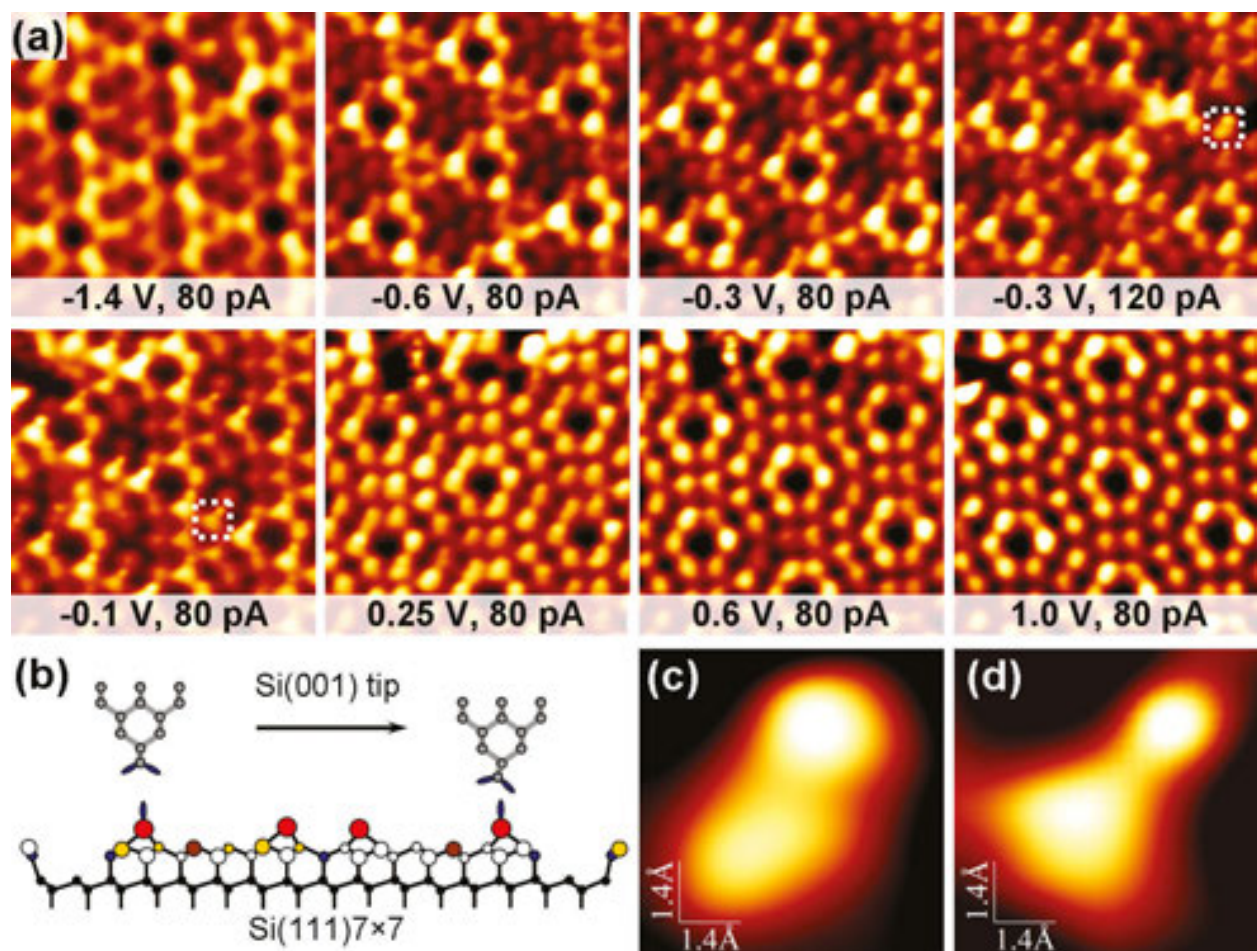

Figure 3. (a) 7.1×7.1 nm^2 STM images of the Si(111)7×7 surface measured at different bias voltages and tunneling currents (shown on each frame) with the silicon-terminated tungsten tip [28]. The fast scanning direction was from left to right. (b) Side view of a [001]-oriented silicon tip over the Si(111)7×7 surface; right panel depicts a tip bending opposite to the scan direction. (c,d) Zooms of the double features indicated by squares on images measured at $U = –0.3$ V, $I = 80$ pA (c) and $U = –0.1$ V, $I = 80$ pA (d).

artifacts [83], presence of a carbon atom at the apex [86], and visualization of the surface atoms' backbonds [87] were proposed. Nevertheless, independent theoretical calculations [31, 32, 82, 84] support the possibility of direct visualization of the asymmetric charge distribution around the [001]-oriented Si tip atom [**Figure 3(b)**] at small (2.5–4.0 Å) tip-surface separations. This is in agreement with the gap-resistance–dependent STM experiments [28]. **Figure 3(a)** demonstrates that the twofold splitting of the adatoms becomes discernible only at small bias voltages (small distances), while at large negative voltages a (7×7) pattern with with well-resolved adatoms, rest atoms, corner holes, and single-atom defects are observed, which is only possible with extremely sharp single atom–terminated tips [88]. The effect can hardly be explained by the formation of a two-atom terminated apex and visualization of the surface atom backbonds because deep corner holes, rest atoms, and single atom defects on the surface were simultaneously resolved even at low gap resistances. The double features become sharper and change their appearance from symmetric to asymmetric with decreasing gap resistance, as shown in **Figure 3 (c)** and **(d)**. The shape of the double features could be changed both by increasing tunneling current at fixed voltage and decreasing voltage at the same current [28]. The asymmetry of the double features at small gaps can be explained by the relaxation of the apex atom, as shown in **Figure 3(b)**. The distance between the two maxima of the double features decreased from 2.7 to 2.2 Å with decreasing gap resistance from 7.5 to 2.5 GΩ and then increased to 2.75 Å with further decreasing gap resistance from 2.5 to 1.25 GΩ. The decrease of the distance between the subatomic maxima is in line with the theoretical spatial distribution of the two sp^3 dangling bonds at the [001]-oriented silicon apex [32]. The increase of the splitting at smaller distances can be related to tip-sample interaction modifying the electronic structure of the apex atom and inducing lateral relaxations of the tip and surface atoms in near-to-contact regime.

Herz et al. applied a Co_6Fe_3Sm tip for high-resolution STM experiments on the Si(111)7×7 surface [25]. They utilized a dynamic-STM mode with an oscillating probe to reduce the lateral forces in tip-sample contact and increase the tip stability at extremely small tunneling gaps. At some tunneling parameters, the adatoms were resolved as extremely sharp spherically symmetric features surrounded by lower lying crescents. These asymmetric features, observed at small gaps, were explained by a convolution of the p_z-orbitals of the surface atoms and the f_z^3-orbital of an Sm atom at the apex tilted to the surface normal by 37°. The validity of this interpretation was supported by the theoretical calculations in an assumption of the tilted Sm f_z^3 tip orbital [25].

3.2. d_{yz} electron orbital of a MnNi tip resolved in STM experiments on the Cu(014)–O surface

Figure 4(a) shows the STM image of the Cu(014)–O surface measured using a polycrystalline MnNi tip [26, 27]. The image demonstrates regular twofold splitting of the copper atomic features along the [1–10] direction. The experimental image displays the 7.2±0.2 Å wide terraces, step edges along the [100] direction and an additional fine structure within the terraces. The image reveals a single atom defect proving the sharpness of the MnNi tip. The doubling of atomic features was observed in rare experiments at small negative bias voltages between -30 and -50 mV in a very narrow range of the tunneling currents. That was explained

by the distance dependence of the Cu(014)–O STM images and strong dependence of the tip's electronic structure on the crystallographic orientations of the apex [26, 27].

Figure 4(b) shows the partial density of electron states (PDOS) associated with the Ni and Mn atoms at the apexes of the [001]- and [111]-oriented MnNi tips. The tight binding (TB) calculations demonstrate domination of the d_{yz}-orbital near the Fermi level only for the [111]-oriented MnNi tip terminated by an Mn atom [**Figure 4(b)**]. The density functional theory (DFT) calculations shown in **Figure 4(c)** demonstrate that only certain configurations of the Mn-terminated MnNi[111] tips could produce regular doubling with almost symmetric twofold split features [27]. The regular pattern of the double features reproducing the shape of the Mn atom d_{yz} electron orbital could be resolved when the Cu(014)–O surface d_z^2-orbitals and the tip d_{yz}-orbital provided major contribution to the tunneling current. This is schematically shown in **Figure 4(a)**.
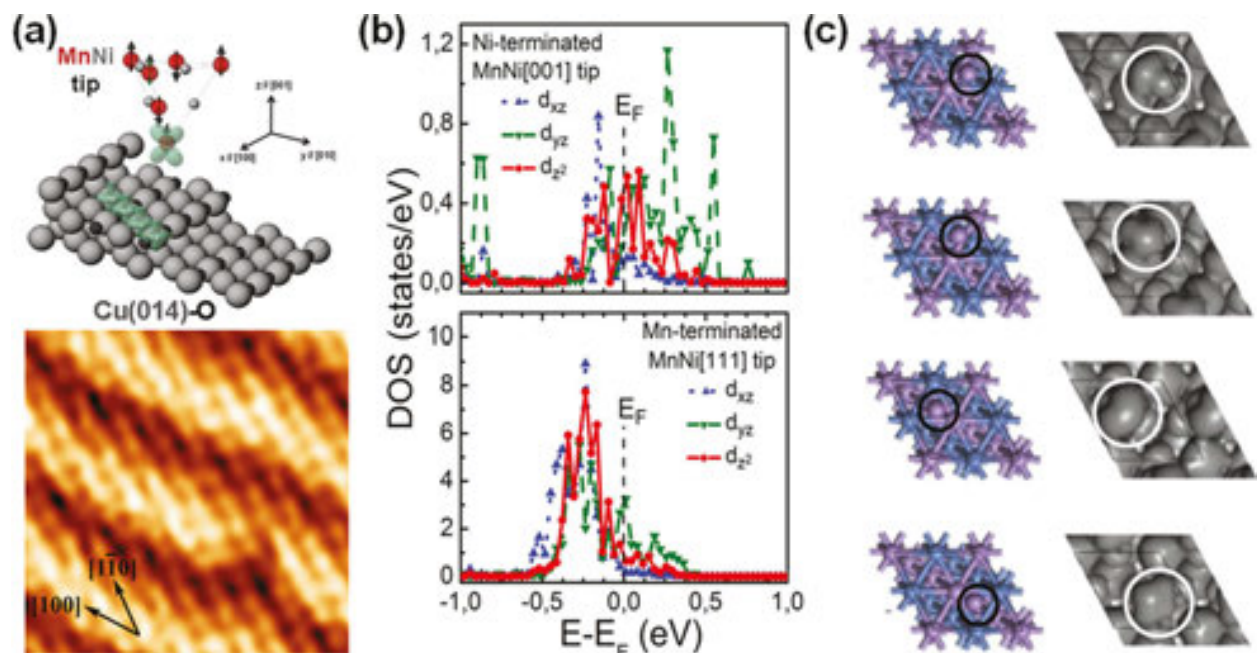

Figure 4. (a) Regular doubling of atomic features in STM images of the Cu(014)–O surface measured with a MnNi tip (bottom) and schematic model of the d_{yz} tip orbital scanning over d_z^2 surface orbitals (top). Eight instead of four features are resolved along the [1–10] direction within each terrace. The image was taken at U = -30 mV and I = 80 pA. (b) PDOS associated with the d-orbitals of the Ni-terminated MnNi[001] tip (top) and Mn-terminated MnNi[111] tip (bottom). (c) Models (left) and calculated electron density isosurfaces (right) for different MnNi[111] tip configurations. The isosurfaces display the electron density at 2.4 × 10⁻³ electrons per Å³ in the E_F ± 0.22 eV energy range. The apex atom is indicated by circles. Reproduced from Reference [27] with permission of APS.

3.3. Distance dependence of the W[001] tip orbital contribution in STM experiments on graphite

The selection of the tip orbital responsible for high-resolution STM imaging has been demonstrated in references [22–24]. The electron orbitals of the graphite surface atoms were used to study the relative contribution of the [001]-oriented single crystalline tungsten tip

orbitals at different distances (**Figure 5**). To avoid apex contamination, W[001] tips were cleaned by flash heating and ion sputtering in ultra-high vacuum (UHV) before the distance-dependent experiments. The transmission electron microscopy (TEM) studies proved the fabrication of the [001]-oriented nanopyramids with well-defined structure at the apexes [24].
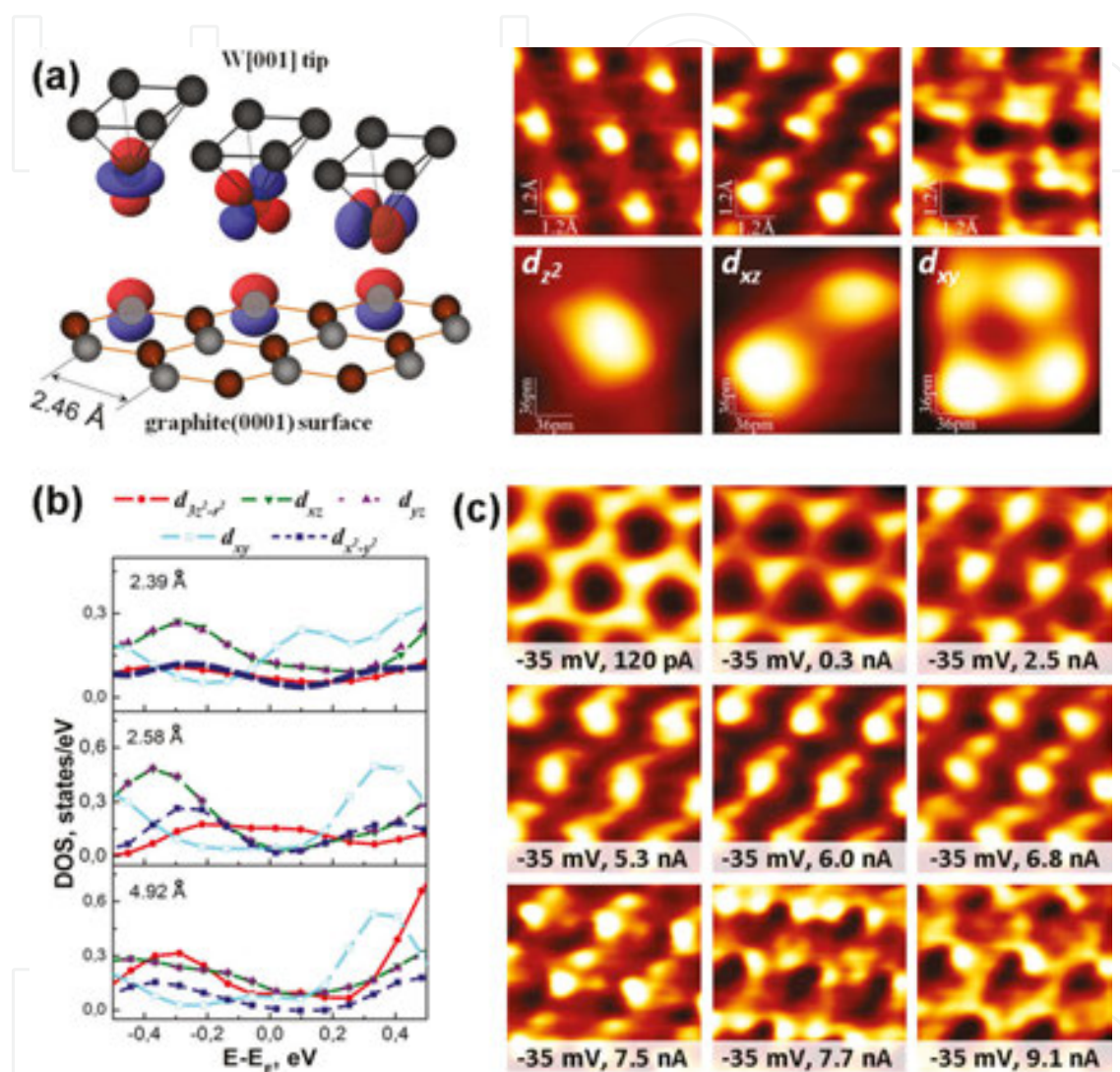

Figure 5. (a) Left: schematic model of a [001]-oriented W tip over a graphite (0001) surface. Right: 6 × 6 Å² (top) and 1.8 × 1.8 Å² (bottom) STM images measured with the W[001] tips at U = 23 mV and I = 2.7 nA (left panels), U = –35 mV and I = 7.4 nA (central panels), U = –100 mV and I = 1.7 nA (right panels). (b) PDOS associated with different d-orbitals of the W[001] tip atom interacting with the graphite (0001) surface. The distances between interacting tip and surface atom nuclei are indicated on each panel. (c) Gap resistance dependence of graphite (0001) STM images measured using a W[001] tip at U = –35 mV. Tunneling currents are indicated on each frame. Panel (b) is reproduced from reference [23] with permission of Elsevier.

Figure 5(c) shows a gap resistance dependence measured with a W[001] tip at a bias voltage of −35 mV. At smaller currents (larger distances) a hexagonal pattern is observed. The atomic features become sharper with increasing tunneling current (decreasing distance). With further increase in the tunneling current, the symmetric features are transformed into two, three, and

fourfold split subatomic features at currents between 5.3 and 9.1 nA. Similar subatomic features were earlier observed in AFM experiments with polycrystalline tungsten probes [33] and ascribed to the orbital structure of the tungsten tips with three different crystallographic orientations. The gap resistance dependence measured with the unchanged W[001] tip [**Figure 5(c)**] demonstrates that these images reproduce the electronic structure of the same tip atom modified with decreasing tip-sample distance. The two and fourfold split features in **Figure 5** cannot correspond to the threefold symmetrical graphite surface. At the same time, the observed two and threefold split features cannot be related to the tip atom backbonding because of the symmetry of the W[001] tip used in experiments. The subatomic features can only be explained by a direct visualization of the tip atom's electronic structure modified by the tip-sample interaction at small tunneling gaps. According to the tunneling currents, the observed transformation of the asymmetric features took place in the narrow range of tip-sample distances of the order of 0.1 Å. The actual distance could be slightly above this value because of the tip and surface atom relaxations at small distances [37].

At certain tunneling parameters (voltages and gap resistances), the shapes of the subatomic features in the STM experiments reproduced the electron density distribution associated with the d_z^2-, d_{xz}-, and d_{xy}-orbitals in the tungsten atom. This can be explained by a major contribution of particular electron orbitals of the tip atom at certain tip-sample distances [**Figure 5(a)**]. According to **Figure 5(c)**, the relative contribution of the d_{xz}- and d_{xy}-orbitals increases with decreasing gap resistance. PDOS calculations for the fully relaxed "W[001] tip–graphite" system [**Figure 5(b)**] demonstrate a suppression of the tip d_z^2 electron orbital near E_F at distances below 2.5 Å because of the overlap with the carbon orbitals. The domination of the tip d_{xy} electron orbital near E_F is observed in a narrow range of the tip-surface distances between 2.2 and 2.5 Å, which is in agreement with the current values in **Figure 5(c)**. The surface imaging by the tungsten d_z^2-orbital can be realized at tunneling gaps between 2.5 and 4.0 Å, while d_{xy} electron orbital can yield a maximum contribution to the tunneling current at distances between 2.2 and 2.5 Å. The appearance of the asymmetric features is related to the interaction-induced modification of the PDOS associated with different d-orbitals of the tungsten tip atom.

The DFT calculations [**Figure 5(b)**] and distance-dependent STM experiments [**Figure 5(c)**] show the correlation between the spatial distribution of the atomic orbitals (in particular, extension in the z-direction) and the order of their suppression with decreasing tip-sample distance. The suppression of the further protruded in the z-direction electron orbitals with $m = 0$ can increase the contribution of the $m \neq 0$ electron states at small gaps. **Figure 5** demonstrates that picoscale spatial resolution and even direct imaging of the transition metal d-orbitals using the p-orbitals of light elements can experimentally be achieved.

3.4. d_{xz}-orbitals of the surface atoms resolved using tungsten tips

STM images shown in **Figures 3–5** correspond to probing the tip electronic structure by the surface atomic orbitals. Similar STM experiments revealing the tip atom's subatomic structure with decreasing tunneling gap have recently been reported for several tip-sample systems [89–92]. **Figure 6(a)** shows the STM image of the Cu(014)–O surface measured with a polycrystal-line tungsten tip [30]. This image reveals one bright atomic row within the four-atom-wide

terraces [see the model in **Figure 4(a)**]. The atomic features within the well-resolved copper row have two maxima separated by approximately 1 Å [**Figure 6(b)**] reproducing the electron density distribution in the Cu d_{xz} atomic orbital. According to the TB calculations [**Figure 6(c)**], the DOS associated with the d_{xz}-orbitals of the surface copper atoms is maximal for the fourth (down-step) copper row of each terrace suggesting that visualization of one atomic row within the terraces can be achieved if the surface d_{xz}-orbitals yield the largest contribution to the tunneling current. Similar to the STM experiments with the W[001] tips [22–24], this can be reached at small bias voltages and small tip-sample distances, where the d_{xz}-orbital channel dominates in the tunneling current. The STM image with one well-resolved row with double features (**Figure 6(a)**) can be explained by imaging the d_{xz}-orbitals of the Cu(014)–O surface using the d_z^2-orbital of a tungsten tip atom.
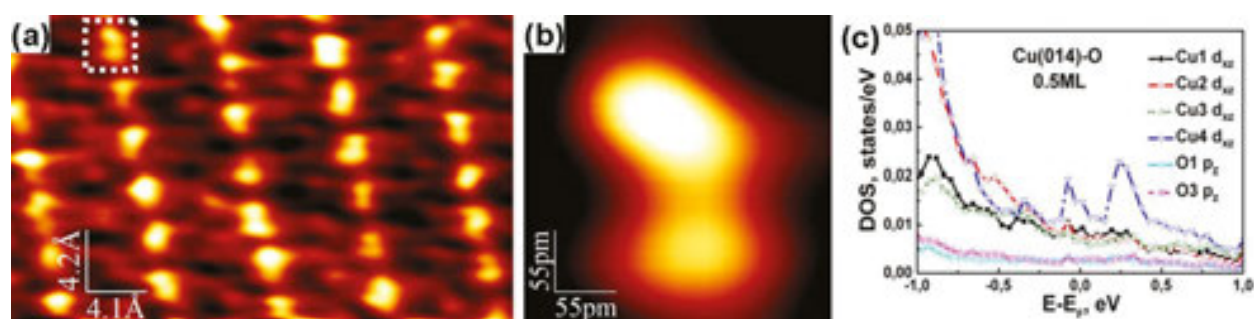

Figure 6. (a) A 3.4×2.1 nm² STM image of the Cu(014)–O surface illustrating the asymmetry of the atomic features associated with the down-step copper row resolved using a polycrystalline W tip at U = –5 mV and I = 0.1 nA [30]. (b) A 2.8×2.8 Å² STM image of a subatomic feature reproducing the shape of the Cu d_{xz} electron orbital. (c) PDOS associated with the Cu d_{xz}-orbitals and O p_z-orbitals of the Cu(014)–O surface. The model of the surface is shown in **Figure 4(a)**.

3.5. STM imaging of graphite (0001) using a [111]-oriented diamond tip

Conductive diamond tips, generally considered as AFM probes, can provide carbon atomic orbitals for imaging with picometer lateral resolution (**Figure 5**) and high apex stability at small tunneling gaps. It has been demonstrated that high spatial resolution can be achieved in STM experiments with the boron-doped single crystal diamond tips [93]. **Figure 7(a)–(d)** displays a comparison of the spatial resolution achieved with the [111]-oriented diamond and [001]-oriented tungsten probes. Note that image in **Figure 7(b)** was measured with the W[001] tip used for the high-resolution experiments on graphite (**Figure 5**) and surfaces with nontrivial atomic and electronic structures [94, 95]. The images taken with the diamond and W[001] probes [**Figure 7(a)** and **(b)**] reveal two sublattices corresponding to nonequivalent α and β atoms in the honeycomb lattice. However, the hollow sites are substantially deeper and individual surface atoms are better resolved in the image measured with the diamond probe, as the cross-sections in **Figure 7(c)** and **(d)** illustrate. DFT calculations [93] showed that the DOS at E_F is larger by approximately 25% for β atoms [**Figure 7(f)**] and the difference decreases for the DOS integrated over a wider range of the electron energies. That explains the two slightly nonequivalent sublattices in **Figure 7(a)** and **(b)**. The smaller height difference between

the features corresponding to α and β atoms for the image measured at $U = -0.4$ V [**Figure 7(b)**] is in agreement with the decreasing difference in the DOS at larger energies.

Figure 7(g) and **(h)** shows the experimental STM image resolved with the diamond tip and the calculated charge density map corresponding to the surface electron states near E_F, respectively. Both images demonstrate different contrast on α and β atoms. The DOS shown in **Figure 7(e, f)** and the charge density map presented in **Figure 7(g)** were calculated at a tip-sample distance of 4.5 Å where the atomic and electronic structures of the tip and surface atoms are not substantially modified by the interaction [93]. The excellent agreement between experimental and theoretical images suggests that the highest resolution was achieved with the diamond probe at tunneling gaps of 3.5–4.5 Å where the tip did not strongly interact with the surface. This result shows the advantages of the oriented single crystal diamond probes: their structure is stable and well defined while high lateral and vertical resolution can be achieved at larger tunneling gaps comparing to typical tip-sample distances used in experiments with transition metal tips.
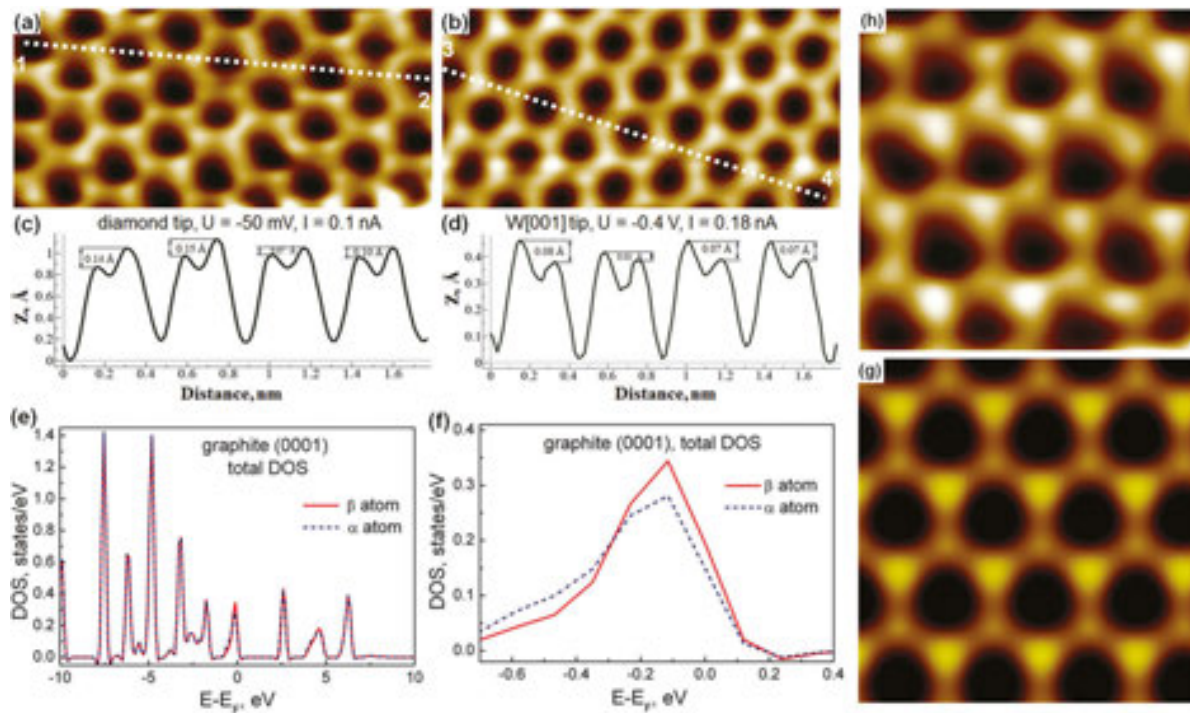

Figure 7. (a, b) 18×9 Å^2 atomically resolved STM images of graphite (0001) measured with a diamond probe at $U = -50$ mV and $I = 0.1$ nA (a) and a W[001] probe at $U = -0.4$ V and $I = 0.18$ nA (b). (c, d) Cross sections 1–2 (c) and 3–4 (d) of the images in panels (a) and (b), respectively. (e, f) Total DOS associated with the α and β atoms of a graphite (0001) surface. (g, h) Comparison of the 9×9 Å^2 calculated electron density distribution map in the energy range from $E_F - 0.2$ eV to E_F (g) and the experimental STM image measured with the diamond probe at $U = -50$ mV and $I = 0.8$ nA (h). Both images show nonequivalence of the α and β atoms in accordance with the DOS shown in panels (e) and (f). Reproduced from Reference [93] with permission of IOP.

Calculations of the partial DOS associated with the electron orbitals of the diamond probe and graphite surface atoms at different tunneling gaps (**Figure 8**) show that electronic structure of the interacting atoms is modified at tip-sample distances below 3.0 Å. The overlap of the tip

and surface atomic orbitals leads to decrease in the PDOS associated with the p_z-orbital of the graphite surface atoms when the diamond tip atom is positioned directly above the surface atom [**Figure 7**(**a**, right panel)]. The suppression of the surface atom's p_z-orbital at small tunneling gaps ($d < 2.5$ Å) is in qualitative agreement with the results of the theoretical calculations for the Si(111)7×7 surface interacting with the W[001] tip shown in **Figure 2** [78]. If the diamond tip atom is positioned above the hollow site (left panels in **Figure 8**), the overlap of the front tip atom and the surface orbitals does not take place even at small distances. Therefore, the change of the PDOS of the tip and surface atoms is minor even at the tunneling gaps of 1.5 Å. According to the calculations [93], the electronic structure of the diamond probe is defined by a mixture of the carbon s and p-states with domination of the p_x- and p_y-orbitals, responsible for the STM imaging (**Figure 7**).
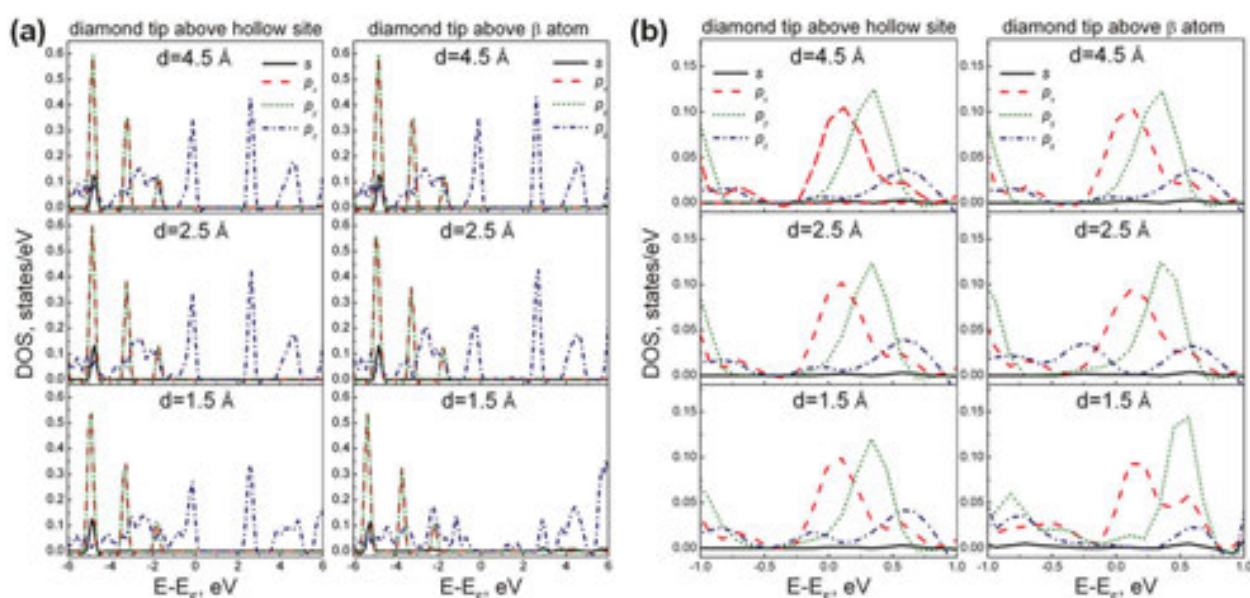

Figure 8. Partial DOS of the β atom of a graphite (0001) surface closest to the diamond tip (a) and the tip apex atom (b) at different tunneling gaps and lateral positions of the tip. Reproduced from Reference [93] with permission of IOP.

3.6. STM experiments with functionalized tips terminated by a light element atom

The experiments with the diamond tip (**Figure 7**) show that an enhancement of the spatial resolution can be achieved using conductive tips having molecules or light element atom at the apex. During the recent years, a number of high-resolution STM studies performed with the conductive tips functionalized by different light elements have been reported [57–59, 89, 96–103]. These studies generally demonstrated an enhanced contrast in the STM experiments with the light element–terminated probes, especially, at small tip-surface distances. For example, the lateral resolution at the level of intramolecular chemical bonds has been reached in STM experiments using molecule-terminated probes [58, 59]. In the recent theoretical work [101], the high resolution in experiments with the functionalized probes was explained by

significant apex atom relaxations toward the local minima of the interaction potential at small distances. However, the tip functionalization procedures are generally not capable of producing stable apexes with well-defined structure. These tips could produce substantial noise [58] and asymmetric subatomic features [89] at small tunneling gaps. Besides, STM images measured with the molecule-terminated tips can strongly depend on the precise orientation of the molecule at the apex and the bias voltage [102, 103] that can complicate the interpretation of the atomically resolved STM data.

3.7. STM imaging of the random bond length distortions in graphene using a W[111] tip

Figure 9 demonstrates the picometer lateral resolution achieved in high-resolution STM studies of graphene/SiC(001) system [7] using a [111]-oriented single crystalline tungsten tip. Theoretical calculations shown in **Figure 1** suggest that the front atom of the W[111] tip should possess symmetric charge distribution along the tip axis even at small tip-sample distances. Although the W[111] tips were found to be the least stable from three possible low-index crystallographic orientations [75], they can produce higher spatial resolution in STM experiments without possible tip structure effects which can be observed with the W[001] tips (**Figure 5**). Indeed, although high spatial resolution was achieved on the quasi-freestanding graphene grown on SiC(001) with the stable W[001] tips [24], the best resolution was obtained with the W[111] tip [7]. **Figure 9(a)** demonstrates the rippled morphology of graphene on SiC(001) with the lateral and vertical dimensions of the ripples of about 30–50 and 1 Å, respectively. **Figure 9(b)** and **(c)** demonstrates random picoscale distortions of the carbon bond lengths, which are very close to the values calculated for the freestanding graphene monolayer [104]. The contrast in **Figure 9(b)** and **(c)** was adjusted to enhance the picometer scale bond length distribution. The picometer lateral resolution obtained in the RT STM experiments (**Figure 9**) corresponds to the best standards of the SPM and can be compared with the resolution achieved in the recent AFM experiments [96].
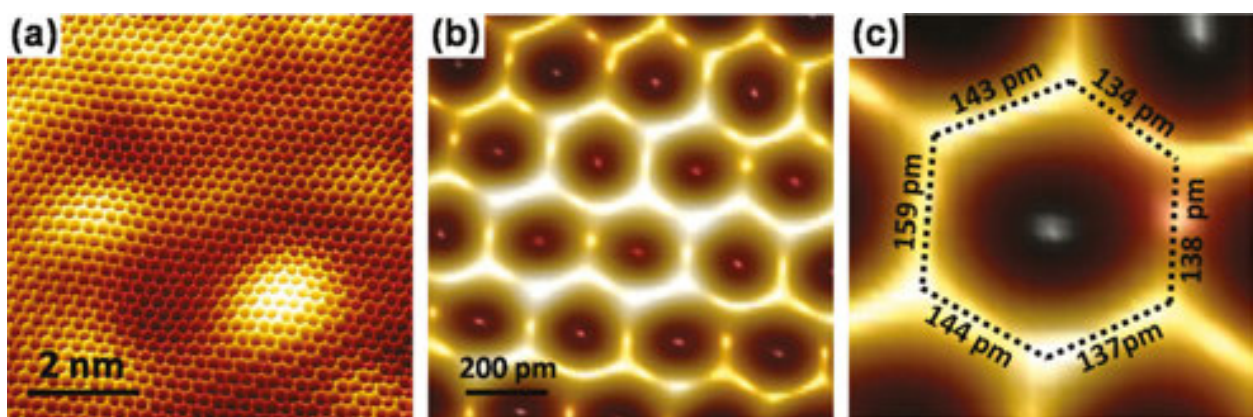

Figure 9. STM images of the graphene synthesized on SiC(001) demonstrating atomic scale rippling (a) and random picoscale distortions of the carbon bond lengths in the graphene lattice (b, c). A distorted hexagon is overlaid on the image on panel (c); the size of the hexagon sides is indicated for clarity. The STM images were measured at U = 22 mV and I = 70 pA (a); U = 22 mV and I=65 pA (b, c).

4. Conclusions

The spatial resolution on the level of individual electron orbitals corresponds to the ultimate resolution of the SPM. During the last decade, a number of SPM studies demonstrating selective visualization of individual electron orbitals and subatomic contrast have been published. The experimental and theoretical works conducted during the recent years demonstrate that selective imaging of the surface electron orbitals can only be achieved at finely adjusted bias voltages and tip-sample distances. Therefore, for the development of the electron orbital imaging capability, the stability of the tip-sample separation should be maintained at the level of 1 pm or below. Distance-dependent STM imaging with electron orbital resolution can lead to further improvement of the lateral resolution down to the picometer scale and development of the chemical-selective imaging of complex multicomponent surfaces.

Acknowledgements

Author details

Alexander N. Chaika

Address all correspondence to: chaika@issp.ac.ru

Institute of Solid State Physics, Russian Academy of Sciences, Chernogolovka, Russia

References

[1] Binnig G, Rohrer H, Gerber C, Weibel E. Tunneling through a controllable vacuum gap. Appl. Phys. Lett. 1982;40:178–180. doi:10.1063/1.92999.

[2] Binnig G, Rohrer H. Scanning tunnelling microscopy. Helv. Phys. Acta 1982;55:726–735. doi:10.5169seals-115309.

[3]   Binnig G, Quate CF, Gerber C. Atomic force microscope. Phys. Rev. Lett. 1986;56:930–933. doi:10.1103/PhysRevLett.56.930.

[4]   Binnig G, Rohrer H, Gerber C, Weibel E. Surface studies by scanning tunneling microscopy. Phys. Rev. Lett. 1982;49: 57–61. doi:10.1103/PhysRevLett.49.57.

[5]   Binnig G, Rohrer H, Gerber C, Weibel E. (7×7) reconstruction on Si(111) resolved in real space. Phys. Rev. Lett. 1983;50:120–123. doi:10.1103/PhysRevLett.50.120.

[6]   Binnig G, Rohrer H, Gerber C, Weibel E. (111) facets as the origin of reconstructed Au(110) surfaces, Surf. Sci. 1983;131:L379–L384. doi:10.1016/0039-6028(83)90112-7.

[7]   Chaika AN, Molodtsova OV, Zakharov AA, Marchenko D, Sanchez-Barriga J, Varykhalov A, et al. Continuous wafer-scale graphene on cubic-SiC(001). Nano Res. 2013;6:562–570. doi:10.1007/s12274-013-0331-9.

[8]   Eigler DM, Schweizer EK. Positioning single atoms with a scanning tunneling microscope. Nature 1990;344:524–526. doi:10.1038/344524a0.

[9]   Crommie MF, Lutz CP, Eigler DM. Confinement of electrons to quantum corrals on a metal surface. Science 1993;262:218–220. doi:10.1126/science.262.5131.218.

[10] Stroscio JA, Celotta RJ. Controlling the dynamics of a single atom in lateral atom manipulation. Science 2004;306:242–247. doi:10.1126/science.1102370.

[11] Walsh MA, Hersam MC. Atomic-scale templates patterned by ultrahigh vacuum scanning tunnelling microscopy on silicon. Annu. Rev. Phys. Chem. 2009;60:193–216. doi:10.1146/annurev.physchem.040808.090314.

[12] Khajetoorians AA, Wiebe J, Chilian B, Wiesendanger R. Realizing all-spin–based logic operations atom by atom. Science 2012;332:1062–1064. doi:10.1126/science.

[13] Khajetoorians AA, Wiebe J, Chilian B, Lounis S, Blügel S, Wiesendanger R. Atom-by-atom engineering and magnetometry of tailored nanomagnets. Nat. Phys. 2012;8:497–503. doi:10.1038/nphys2299.

[14] Krasnikov SA, Lübben O, Murphy BE, Bozhko SI, Chaika AN, Sergeeva NN, et al. Writing with atoms: oxygen adatoms on the MoO_2/Mo(110) surface. Nano Res. 2013;6:929–937. doi:10.1007/s12274-013-0370-2.

[15] Gawronski H, Mehlhorn M, Morgenstern K. Imaging phonon excitation with atomic resolution. Science 2008;319:930–933. doi:10.1126/science.1152473.

[16] Stipe BC, Rezaei MA, Ho W. Single-molecule vibrational spectroscopy and microscopy. Science 1998;280:1732–1735. doi:10.1126/science.280.5370.1732.

[17] Feenstra RM, Stroscio JA, Tersoff J, Fein AP. Atom-selective imaging of the GaAs(110) surface. Phys. Rev. Lett. 1987;58:1192–1195. doi:10.1103/PhysRevLett.58.1192.

[18] Schmid M, Stadler H, Varga P. Direct observation of surface chemical order by scanning tunneling microscopy. Phys. Rev. Lett. 1993;70:1441–1444. doi:10.1103/PhysRevLett. 70.1441.

[19] Wiesendanger R, Güntherodt HJ, Güntherodt G, Gambino RJ, Ruf R. Observation of vacuum tunneling of spin-polarized electrons with the scanning tunneling microscope. Phys. Rev. Lett. 1990;65:247–250. doi:10.1103/PhysRevLett.65.247.

[20] Wiesendanger R, Shvets IV, Bürgler D, Tarrach G, Güntherodt HJ, Coey JMD, Gräser S. Topographic and magnetic-sensitive scanning tunneling microscope study of magnetite. Science 1992;255:583–586. doi:10.1126/science.255.5044.583.

[21] Wiesendanger R. Spin mapping at the nanoscale and atomic scale. Rev. Mod. Phys. 2009;81:1495–1550. doi:10.1103/RevModPhys.81.1495.

[22] Chaika AN, Nazin SS, Semenov VN, Bozhko SI, Lübben O, Krasnikov SA, et al. Selecting the tip electron orbital for scanning tunneling microscopy imaging with sub-Ångström lateral resolution. EPL 2010;92:46003. doi:10.1209/0295-5075/92/46003.

[23] Chaika AN, Nazin SS, Semenov VN, Orlova NN, Bozhko SI, Lübben O, et al. High resolution STM imaging with oriented single crystalline tips. Appl. Surf. Sci. 2013;267:219–223. doi:10.1016/j.apsusc.2012.10.171.

[24] Chaika AN, Orlova NN, Semenov VN, Postnova EYu, Krasnikov SA, Lazarev MG, et al. Fabrication of [001]-oriented tungsten tips for high resolution scanning tunneling microscopy. Sci. Rep. 2014;4:3742. doi:10.1038/srep03742.

[25] Herz M, Giessibl FJ, Mannhart J. Probing the shape of atoms in real space. Phys. Rev. B 2003;68:045301. doi:10.1103/PhysRevB.68.045301.

[26] Chaika AN, Semenov VN, Nazin SS, Bozhko SI, Murphy S, Radican K, Shvets IV. Atomic row doubling in the STM images of Cu(014)-O obtained with MnNi tips. Phys. Rev. Lett. 2007;98:206101. doi:10.1103/PhysRevLett.98.206101.

[27] Murphy S, Radican K, Shvets IV, Chaika AN, Semenov VN, Nazin SS, Bozhko SI. Asymmetry effects in atomically resolved STM images of Cu(014)-O and W(100)-O surfaces measured with MnNi tips. Phys. Rev. B 2007;76:245423. doi:10.1103/PhysRevB. 76.245423.

[28] Chaika AN, Myagkov AN. Imaging atomic orbitals in STM experiments on a Si(111)-(7×7) surface. Chem. Phys. Lett. 2008;453:217–221. doi:10.1016/j.cplett.2008.01.025.

[29] Garleff JK, Wenderoth M, Sauthoff K, Ulbrich RG, Rohlfing M. 2×1 reconstructed Si(111) surface: STM experiments versus ab initio calculations. Phys. Rev. B 2004;70:245424. doi:10.1103/PhysRevB.70.245424.

[30] Chaika AN, Nazin SS, Bozhko SI. Selective STM imaging of oxygen-induced Cu(115) surface reconstructions with tungsten probes. Surf. Sci. 2008;602:2078–2088. doi: 10.1016/j.susc.2008.04.014.

[31] Giessibl FJ, Hembacher S, Bielefeldt H, Mannhart J. Subatomic features on the silicon (111)-(7×7) surface observed by atomic force microscopy. Science 2000;289:422–425. doi: 10.1126/science.289.5478.422.

[32] Giessibl FJ, Bielefeldt H, Hembacher S, Mannhart J. Imaging of atomic orbitals with the atomic force microscope—experiments and simulations. Ann. Phys. 2001;10:887–910. doi:10.1002/1521-3889(200111)10:11/12<887::AID-ANDP887=3.0.CO;2-B.

[33] Hembacher S, Giessibl FJ, Mannhart J. Force microscopy with light-atom probes. Science 2004;305:380–383. doi:10.1126/science.1099730.

[34] Fowler RH, Nordheim L. Electron Emission in Intense Electric Fields. Proc. R. Soc. Lond. A 1928;119:173–181. doi:10.1098/rspa.1928.0091.

[35] Bryant A, Smith DPE, Binnig G, Harrison WA, Quate CF. Anomalous distance dependence in scanning tunneling microscopy. Appl. Phys. Lett. 1986;49:936–938. doi: 10.1063/1.97489.

[36] Jurczyszyn L, Mingo N, Flores F. Influence of the atomic and electronic structure of the tip on STM images and STS spectra. Surf. Sci. 1998;402–404:459–463. doi:10.1016/S0039-6028(97)00971-0.

[37] Hofer WA, Garcia-Lekue A, Brune H. The role of surface elasticity in giant corrugations observed by scanning tunneling microscopes. Chem. Phys. Lett. 2004;397:354–359. doi:10.1016/j.cplett.2004.08.110.

[38] Bode M, Pascal R, Wiesendanger R. Distance-dependent STM-study of the W(110)/C-R(15×3) surface. Z. Phys. B 1996;101:103–107. doi:10.1007/s002570050187.

[39] Wiesendanger R, Bode M, Pascal R, Allers W, Schwarz UD. Issues of atomic-resolution structure and chemical analysis by scanning probe microscopy and spectroscopy. J. Vac. Sci. Technol. A 1996;14:1161–1167. doi:10.1116/1.580259.

[40] Klijn J, Sacharow L, Meyer C, Blugel S, Morgenstern M, Wiesendanger R. STM measurements on the InAs(110) surface directly compared with surface electronic structure calculations. Phys. Rev. B 2003;68:205327. doi:10.1103/PhysRevB.68.205327.

[41] Calleja F, Arnau A, Hinarejos JJ, Vazquez de Parga AL, Hofer WA, Echenique PM, Miranda R. Contrast reversal and shape changes of atomic adsorbates measured with scanning tunneling microscopy. Phys. Rev. Lett. 2004;92:206101. doi:10.1103/PhysRevLett.92.206101.

[42] Blanco JM, González C, Jelínek P, Ortega J, Flores F, Pérez R, et al. Origin of contrast in STM images of oxygen on Pd(111) and its dependence on tip structure and tunneling parameters. Phys. Rev. B 2005;71:113402. doi:10.1103/PhysRevB.71.113402.

[43] Woolcot T, Teobaldi G, Pang CL, Beglitis NS, Fisher AJ, Hofer WA, Thornton G. Scanning tunneling microscopy contrast mechanisms for TiO_2. Phys. Rev. Lett. 2012;109:156105. doi:10.1103/PhysRevLett.109.156105.

[44] Mönig H, Todorovic M, Baykara MZ, Schwendemann TC, Rodrigo L, Altman EI, et al. Understanding scanning tunneling microscopy contrast mechanisms on metal oxides: a case study. ACS Nano 2013;7:10233–10244. doi:10.1021/nn4045358.

[45] Ondracek M, Pou P, Rozsıval V, Gonzalez C, Jelınek P, Perez R, Forces and currents in carbon nanostructures: are we imaging atoms? Phys. Rev. Lett. 2011;106:176101. doi: 10.1103/PhysRevLett.106.176101.

[46] Ondracek M, Gonzalez C, Jelınek P. Reversal of atomic contrast in scanning probe microscopy on (111) metal surfaces. J. Phys.: Condens. Matter 2012;24:084003. doi: 10.1088/0953-8984/24/8/084003.

[47] Tersoff J, Hamann DR. Theory and application for the scanning tunneling microscope. Phys. Rev. Lett. 1983;50:1998–2001. doi:10.1103/PhysRevLett.50.1998.

[48] Tersoff J, Hamann DR. Theory of the scanning tunneling microscope. Phys. Rev. B 1985;31:805–813. doi:10.1103/PhysRevB.31.805.

[49] Wintterlin J, Wiechers J, Brune H, Gritsch T, Hofer H, Behm RJ. Atomic-resolution imaging of close-packed metal surfaces by scanning tunneling microscopy. Phys. Rev. Lett. 1989;62:59–62. doi:10.1103/PhysRevLett.62.59.

[50] Hallmark V, Chiang S, Rabalt J, Swalen J, Wilson R. Observation of atomic corrugation on Au(111) by scanning tunneling microscopy. Phys. Rev. Lett. 1987;59:2879–2882. doi: 10.1103/PhysRevLett.59.2879.

[51] Wintterlin J, Brune H, Hofer H, Behm R. Atomic scale characterization of oxygen adsorbates on Al(111) by scanning tunneling microscopy. Appl. Phys. A 1988;47:99–102. doi:10.1007/BF00619706.

[52] Tersoff J, Lang ND. Tip-dependent corrugation of graphite in scanning tunneling microscopy. Phys. Rev. Lett. 1990;65:1132–1135. doi:10.1103/PhysRevLett.65.1132.

[53] Chen CJ. Origin of atomic resolution on metal surfaces in scanning tunneling microscopy. Phys. Rev. Lett. 1990;65:448–451. doi:10.1103/PhysRevLett.65.448.

[54] Chen CJ. Tunneling matrix elements in three-dimensional space: the derivative rule and the sum rule. Phys. Rev. B 1990;42:8841–8857. doi:10.1103/PhysRevB.42.8841.

[55] Chen CJ. Effects of $m \neq 0$ tip states in scanning tunneling microscopy: the explanation of corrugation reversal. Phys. Rev. Lett. 1992;69:1656–1659. doi:10.1103/PhysRevLett. 69.1656.

[56] Sacks W. Tip orbitals and the atomic corrugation of metal surfaces in scanning tunneling microscopy. Phys. Rev. B 2000;61:7656–7668. doi:10.1103/PhysRevB.61.7656.

[57] Temirov R, Soubatch S, Neucheva O, Lassise AC, Tautz FS. A novel method achieving ultra-high geometrical resolution in scanning tunnelling microscopy. New J. Phys. 2008;10:053012. doi:10.1088/1367-2630/10/5/053012.

[58] Weiss C, Wagner C, Kleimann C, Rohlfing M, Tautz FS, Temirov R. Imaging Pauli repulsion in scanning tunneling microscopy. Phys. Rev. Lett. 2010;105:086103. doi: 10.1103/PhysRevLett.105.086103.

[59] Gross L, Moll N, Mohn F, Curioni A, Meyer G, Hanke F, Persson M. High-resolution molecular orbital imaging using a *p*-wave STM tip. Phys. Rev. Lett. 2011;107:086101. doi:10.1103/PhysRevLett.107.086101.

[60] Gross L, Mohn F, Moll N, Schuler B, Criado A, Guitian E, Pena D, Gourdon A, Meyer G. Bond-order discrimination by atomic force microscopy. Science 2012;337:1326–1329. doi:10.1126/science.1225621.

[61] Scheer E, Agrait N, Cuevas JC, Yeyati AL, Ludoph B, Martin-Rodero A, et al. The signature of chemical valence in the electrical conduction through a single-atom contact. Nature 1998;394:154–157. doi:10.1038/28112.

[62] Polok M, Fedorov DV, Bagrets A, Zahn P, Mertig I. Evaluation of conduction eigen-channels of an adatom probed by an STM tip. Phys. Rev. B 2011;83:245426. doi:10.1103/PhysRevB.83.245426.

[63] Choi H, Longo RC, Huang M, Randall JN, Wallace RM, Cho K. A density-functional theory study of tip electronic structures in scanning tunneling microscopy. Nanotechnology 2013;24:105201. doi:10.1088/0957-4484/24/10/105201.

[64] Suominen I, Nieminen J, Markiewicz RS, Bansil A. Effect of orbital symmetry of the tip on scanning tunneling spectra of $Bi_2Sr_2CaCu_2O_{8+\delta}$. Phys. Rev. B 2011;84:014528. doi: 10.1103/PhysRevB.84.014528.

[65] Palotas K, Mandi G, Hofer WA. Three-dimensional Wentzel-Kramers-Brillouin approach for the simulation of scanning tunneling microscopy and spectroscopy. Front. Phys. 2014;9:711–747. doi:10.1007/s11467-013-0354-4.

[66] Palotas K, Mandi G, Szunyogh L. Orbital-dependent electron tunneling within the atom superposition approach: theory and application to W(110). Phys. Rev. B 2012;86:235415. doi:10.1103/PhysRevB.86.235415

[67] Mandi G, Palotas K. STM contrast inversion of the Fe(110) surface. Appl. Surf. Sci. 2014;304:65–72. doi:0.1016/j.apsusc.2014.02.143.

[68] da Silva Neto EH, Aynajian P, Baumbach RE, Bauer ED, Mydosh J, Ono S, Yazdani A. Detection of electronic nematicity using scanning tunneling microscopy. Phys. Rev. B 2013;87:161117. doi:10.1103/PhysRevB.87.161117.

[69] Jurczyszyn L, Stankiewicz B. Interorbital interference in STM tip during electron tunneling in tip–sample system: influence on STM images. Prog. Surf. Sci. 2003;74:185–200. doi:10.1016/j.progsurf.2003.08.014.

[70] Jurczyszyn L, Stankiewicz B. The role of interorbital interference in the formation of STS spectra. Appl. Surf. Sci. 2005;242:70–81. doi:10.1016/j.apsusc.2004.07.066.

[71] Hagelaar JHA, Flipse CFJ, Cerda JI. Modeling realistic tip structures: scanning tunneling microscopy of NO adsorption on Rh(111). Phys. Rev. B 2008;78:161405. doi:10.1103/PhysRevB.78.161405.

[72] Telychko M, Mutombo P, Ondracek M, Hapala P, Bocquet FC, Kolorenc J, et al. Achieving high-quality single-atom nitrogen doping of Graphene/SiC(0001) by ion implantation and subsequent thermal stabilization. ACS Nano 2014;8:7318–7324. doi:10.1021/nn502438k.

[73] Sachse T, Neel N, Meierott S, Berndt R, Hofer WA, Kröger J. Electronic and magnetic states of Mn2 and Mn2H on Ag(111). New J. Phys. 2014;16:063021. doi:10.1088/1367-2630/16/6/063021.

[74] Mandi G, Palotas K. Chen's derivative rule revisited: role of tip-orbital interference in STM. Phys. Rev. B 2015;91:165406. doi:10.103/PhysRevB.91.165406.

[75] Wright CA, Solares SD. Computational study of tip apex symmetry characterization in high-resolution atomic force microscopy. J. Phys. D: Appl. Phys. 2013;46:155307. doi:10.1088/0022-3727/46/15/155307

[76] Wright CA, Solares SD. On mapping sub-Ångström electron clouds with force microscopy. Nano Lett. 2011;11:5026–5033. doi:10.1021/nl2030773.

[77] Wright CA, Solares SD. Imaging of subatomic electron cloud interactions: effect of higher harmonics processing in noncontact atomic force microscopy. Appl. Phys. Lett. 2012;100:163104. doi:10.1063/1.3703767.

[78] Jelınek P, Shvec M, Pou P, Perez R, Chab V. Tip-induced reduction of the resonant tunneling current on semiconductor surfaces. Phys. Rev. Lett. 2008;101:176101. doi:10.1103/PhysRevLett.101.176101

[79] Ternes M, Gonzalez C, Lutz CP, Hapala P, Giessibl FJ, Jelınek P, Heinrich AJ. Interplay of conductance, force, and structural change in metallic point contacts. Phys. Rev. Lett. 2011;106:016802. doi:10.1103/PhysRevLett.106.016802

[80] Neel N, Kröger J, Limot L, Palotas K, Hofer WA, Berndt R. Conductance and Kondo effect in a controlled single-atom contact. Phys. Rev. Lett. 2007;98:016801. doi:10.1103/PhysRevLett.98.016801.

[81] Serrate D, Ferriani P, Yoshida Y, Hla SW, Menzel M, von Bergmann K, et al. Imaging and manipulating the spin direction of individual atoms. Nature Nanotech. 2010;5:350–353. doi:10.1038/nnano.2010.64.

[82] Zotti LA, Hofer WA, Giessibl FJ. Electron scattering in scanning probe microscopy experiments. Chem. Phys. Lett. 2006;420:177–182. doi:10.1016/j.cplett.2005.12.065.

[83] Hug HJ, Lantz MA, Abdurixit A, van Schendel PJA, Hoffmann R, Kappenberger P, Baratoff A. Subatomic features in atomic force microscopy images. Science 2001;291:2509a. doi:10.1126/science.291.5513.2509a.

[84] Huang M, Cuma M, Liu F. Seeing the atomic orbital: first-principles study of the effect of tip termination on atomic force microscopy. Phys. Rev. Lett. 2003;90:256101. doi: 10.1103/PhysRevLett.90.256101.

[85] Chen CJ. Possibility of imaging lateral profiles of individual tetrahedral hybrid orbitals in real space. Nanotechnology 2006;17: S195–S200. doi:10.1088/0957-4484/17/7/S16.

[86] Campbellova A, Ondracek M, Pou P, Perez R, Klapetek P, Jelínek P. "Sub-atomic" resolution of non-contact atomic force microscope images induced by a heterogeneous tip structure: a density functional theory study. Nanotechnology 2011;22:295710. doi: 10.1088/0957-4484/22/29/295710.

[87] Sweetman A, Rahe P, Moriarty P. Unique determination of "subatomic" contrast by imaging covalent backbonding. Nano Lett. 2014;14:2265–2270. doi:10.1021/nl4041803.

[88] Wang YL, Gao HJ, Guo HM, Liu HW, Batyrev IG, McMahon WE, Zhang SB. Tip size effect on the appearance of a STM image for complex surfaces: theory versus experiment for Si(111)-(7×7). Phys. Rev. B 2004;70:073312. doi:10.1103/PhysRevB.70.073312.

[89] Li Z, Schouteden K, Iancu V, Janssens E, Lievens P, van Haesendonck C, Cerdá JI. Chemicaly modified STM tips for atomic-resolution imaging of ultrathin NaCl films. Nano Res. 2015;8:2223–2230. doi:10.1007/s12274-015-0733-y.

[90] Emmrich M, Huber F, Pielmeier F, Welker J, Hofmann T, Schneiderbauer M, et al. Subatomic resolution force microscopy reveals internal structure and adsorption sites of small iron clusters. Science 2015;348:308–311. doi:10.1126/science.aaa5329.

[91] Hofmann T, Pielmeier F, Giessibl FJ. Chemical and crystallographic characterization of the tip apex in scanning probe microscopy. Phys. Rev. Lett. 2014;112:066101. doi: 10.1103/PhysRevLett.112.066101.

[92] Hofmann T, Pielmeier F, Giessibl FJ. Erratum: Chemical and crystallographic characterization of the tip apex in scanning probe microscopy [Phys. Rev. Lett. 112, 066101 (2014)]. Phys. Rev. Lett. 2015;115:109901. doi:10.1103/PhysRevLett.115.109901.

[93] Grushko V, Lubben O, Chaika AN, Novikov N, Mitskevich E, Chepugov A, et al. Atomically resolved STM imaging with a diamond tip: simulation and experiment. Nanotechnology 2014;25:025706. doi:10.1088/09574484/25/2/025706

[94] Chaika AN, Semenov VN, Glebovskiy VG, Bozhko SI. Scanning tunneling microscopy with single crystal W[001] tips: high resolution studies of Si(557)5×5 surface. Appl. Phys. Lett. 2009;95:173107. doi:10.1063/1.3254240.

[95] Yashina LV, Püttner R, Volykhov AA, Stojanov P, Riley J, Vassiliev SY, et al. Atomic geometry and electron structure of the GaTe(1 0 -2) surface. Phys. Rev. B 2012;85:075409. doi:10.1103/PhysRevB.85.075409.

[96]   Gross L, Mohn F, Moll N, Schuler B, Criado A, Guitian E, et al. Bond-order discrimi-nation by atomic force microscopy. Science 2012;337:1326–1329. doi:10.1126/science.1225621.

[97]   Deng ZT, Lin H, Ji W, Gao L, Lin X, Cheng ZH, et al. Selective analysis of molecular states by functionalized scanning tunneling microscopy tips. Phys. Rev. Lett. 2006;96:156102. doi:10.1103/PhysRevLett.96.156102.

[98]   Cheng Z, Du S, Guo W, Gao L, Deng Z, Jiang N, et al. Direct imaging of molecular orbitals of metal phthalocyanines on metal surfaces with an O_2-functionalized tip of a scanning tunneling microscope. Nano Res. 2011;4:523–530. doi:10.1007/s12274-011-0108-y.

[99]   Mohn F, Gross L, Moll N, Meyer G. Imaging the charge distribution within a single molecule. Nature Nanotech. 2012;7:227–231. doi:10.1038/nnano.2012.20.

[100]   Mohn F, Schuler B, Gross L, Meyer G. Different tips for high-resolution atomic force microscopy and scanning tunneling microscopy of single molecules. Appl. Phys. Lett. 2013;102:073109. doi:10.1063/1.4793200.

[101]   Hapala P, Kichin G, Wagner C, Tautz FS, Temirov R, Jelınek P. Mechanism of high-resolution STM/AFM imaging with functionalized tips. Phys. Rev. B 2014;90:085421. doi:10.1103/PhysRevB.90.085421.

[102]   Chiutu C, Sweetman AM, Lakin AJ, Stannard A, Jarvis S, Kantorovich L, et al. Precise orientation of a single C60 molecule on the tip of a scanning probe microscope, Phys. Rev. Lett. 2012;108:268302.doi:10.1103/PhysRevLett.108.268302.

[103]   Lakin AJ, Chiutu C, Sweetman AM, Moriarty P, Dunn JL. Recovering molecular orientation from convoluted orbitals. Phys. Rev. B 2013;88:035447. doi:10.1103/PhysRevB.88.035447.

[104]   Fasolino A, Los JH, Katsnelson MI. Intrinsic ripples in graphene. Nature Mater. 2007;6:858–861. doi:10.1038/nmat2011.